3-D-MIMO With Massive Antennas Paves the Way to 5G Enhanced Mobile Broadband: From System Design to Field Trials

Guangyi Liu, *Member, IEEE*, Xueying Hou, Jing Jin, Fei Wang, Qixing Wang, Yue Hao, Yuhong Huang, Xiaoyun Wang, Xiao Xiao, and Ailin Deng

***Abstract*— Three-dimensional (3D) multiple input and multiple output (3D-MIMO) with massive antennas is a key technology to achieve high spectral efficiency and user experienced data rate for the fifth generation (5G) mobile communication system. To implement 3D-MIMO in 5G system, practical constraints on the product design should be considered. This paper proposes a systematic design for the 3D-MIMO product by considering the restrictions of both base band and the hardware, including cost, size, weight, and heat dissipation. The design has been implemented for 2.6-GHz time-division duplex band, and field trials have been conducted for performance validation with practical intercell interference in commercial network. The trial results show that this 3D-MIMO design can meet the spectral efficiency requirement of the 5G enhanced mobile broadband services. The performance gain of 3D-MIMO varies with the traffic load. When the traffic load is heavy, 3D-MIMO can enhance the cell throughput by 4∼6.7 times. When the traffic load is low, the performance gain of this 3D-MIMO design decreases. The results from field trial also show that the performance of 3D-MIMO degrades in mobility scenarios, where further enhancement on acquiring instant channel status information are necessary to improve the robustness of 3D-MIMO to mobility.**

***Index Terms*— 3D-MIMO, massive antennas, system-level evaluation, field trial, 5G, eMBB.**

I. Introduction

With rapid development of the 4th Generation mobile communication system (4G) and increasing penetration of smart phones, an explosive growth of mobile data traffic has been witnessed in recent years. On one hand, new services and applications impose high requirements on data rate of mobile network, such as higher resolution videos, glasses-free three-dimension (3D) video, augmented-reality (AR) and virtual-reality (VR) applications. On the other hand, the rapid develop of the Internet-of-Things (IoT) industry increase the number of connections in the mobile network significantly. It will be more and more challenging for the 4G network to meet the ever-increasing demands of mobile broadband traffic and the number of connections. To meet the more stringent and unprecedented requirements, the 5th Generation mobile communications (5G) system is on the way, and it has been attracting growing attentions and efforts in both academia and industry [1].

According to the research of International Telecommunication Union (ITU) [2], the usage scenarios of 5G systemW can be categorized into enhanced Mobile Broadband (eMBB), Ultra-Reliable and Low Latency Communication (URLLC) and massive Machine-Type Communication (mMTC). The requirements on the Key Performance Indicators (KPI) have been defined as [2],

- Peak data rate: 10 Gbps
- User experienced data rate: around 100 Mbps
- Spectral efficiency: 3 times of 4G
- Latency: 1 ms over-the-air latency
- Mobility: up to 500 km/h
- Energy efficiency: not be greater than IMT networks deployed today
- Traffic volume density: 10 Mbps/m^2

Among these requirements, the user experienced data rate and spectral efficiency are two most important KPIs for eMBB network. To meet these two requirements, massive Multiple Input and Multiple Output (Massive MIMO) is identified as a key technology, and is regarded as one of the most important technologies of 5G. It uses a very large number of antenna elements at the base station, which is believed to improve the spectral efficiency greatly through high-order spatial multiuser (MU) multiplexing.

Distributing the massive antenna elements into planar array is a feasible way to reduce the antenna panel size in practical deployment, and such design is dubbed 3D-MIMO, which can exploits both vertical and horizontal domain beamforming for signal transmission. Such enhanced spatial resolution in 3D space helps to improve the desired signal power in expected direction and reduce the inter-cell interference to other directions.

The 3D-MIMO can be applied for both centimeter-wave (cmWave) bands (e.g, sub-6GHz) [3] and

Manuscript received December 15, 2016; revised March 22, 2017; accepted March 22, 2017. Date of publication March 29, 2017; date of current version June 1, 2017. *(Corresponding author: Xueying Hou.)*

G. Liu, X. Hou, J. Jin, F. Wang, Q. Wang, Y. Hao, Y. Huang, and X. Wang are with China Mobile Communication Corporation, Beijing 100053, China (e-mail: liuguangyi@chinamobile.com; houxueying@chinamobile.com; jinjing@chinamobile.com; wangfei@chinamobile.com; haoyue@chinamobile.com; huangyuhong@chinamobile.com; wangxiaoyun@chinamobile.com).

X. Xiao and A. Deng are with Huawei Technologies Co. Ltd., Shenzhen 518129, China (e-mail: george.xiao@huawei.com; dengailin@huawei.com).

Color versions of one or more of the figures in this paper are available online at http://ieeexplore.ieee.org.

Digital Object Identifier 10.1109/JSAC.2017.2687998

millimeter-wave (mm-wave) bands (e.g., above 10GHz) [4]. The cmWave bands are prevalent used by International Mobile Telecommunications (IMT) systems, owing to their superior performance in coverage. The mm-wave bands have attracted great attention recently, since the wide bandwidth available within these bands can be exploited to empower super-high data rate. Considering that wide and seamless coverage still be the fundamental goal for 5G deployment, the 3D-MIMO design for cm-wave bands are targeted in this paper.

To exploit potential benefits of 3D-MIMO in 5G Systems, great efforts have been made in academia, from information theory analysis to implementation issues related to channel model, channel estimation, detection and precoding schemes [5]–[15]. Nonetheless, from academic study to product, 3D-MIMO still has a long way to go to resolve the challenges of both baseband implementation and hardware architecture. In addition, realistic field trials are also necessary to verify the performance gain. Some preliminary studies have been made on the performance validation of 3D-MIMO [16]–[19]. In these studies, the promising gain of 3D-MIMO has been identified. However, the performance gain described are either obtained by simulation with a realistic city-scale 3D ray-tracing channel model [16], or by specially built experimental trial [17]–[19], where the practical inter-cell interference were not addressed. In addition, the test UEs are placed at fixed locations, which means the impact of mobility of UEs is ignored. Moreover, experimental burst traffic pattern is adopted in these papers, which can not fully characterize the various traffic types in commercial network.

In this paper, a systematic design for 3D-MIMO is proposed, and the performance of 5G system with this 3D-MIMO design is verified by both system-level simulations and field trials that conducted in a real network environment. The antenna array selection, Active Antenna System (AAS) architecture, precoding algorithm and traffic adaption scheduling are investigated for practical implementation.

1) We study the tradeoff between performance and implementation complexity of 3D-MIMO with massive antennas, in terms of scheduling, precoding and CSI acquisition based on reciprocity of TDD. Different from the analysis and trials in [16]–[19], where unrealistic full buffer traffic or non-full buffer traffic with the same packet size for all UEs, the analysis herein consider real traffic model in the commercial network, which includes various traffic types with different packet sizes. Practical constraints such as computational capabilities of hardware in current stage are also considered, which helps to explain the gap between theoretical and practical performance of 3D-MIMO systems.
2) We also propose the hardware design of 3D-MIMO with massive antennas, including both hardware architecture and antenna placement, where compromises are made between performance gain and practical constraints. Based on the analysis, a promising hardware and antenna architecture is proposed, which helps to accelerate the deployment and commercialization for 3D-MIMO with massive antennas in 5G systems.

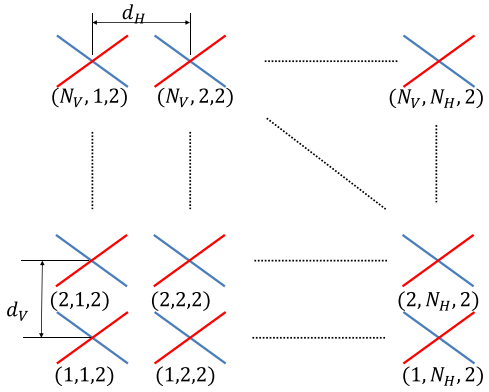

Fig. 1. Antenna array structure, which is denoted by (N_{V},N_{H}, N_{P}). N_{H} is the number of columns, N_{V} is the number of antenna elements with the same polarization in each column, and $N_{\mathrm{P}} = 2$ is the number of polarization dimensions.

3) Based on the proposed implementation algorithms and hardware architecture mentioned above, the performance of 3D-MIMO with massive antennas are evaluated in field trials with real-time traffic and inter-cell interference. The results obtained from field trials confirm the superior performance of 3D-MIMO in improving the spectral efficiency and capacity. It is shown that by exploiting 3D-MIMO with massive antennas, the spectral efficiency and throughput requirements of 5G systems can be satisfied. In addition, the test results also reveal that, assuming 5G uses the existing LTE physical layer design, the 3D-MIMO performance degrades with increasing mobility and only limited coverage gain can be achieved. Therefore, it is necessary to develop further enhancements for 3D-MIMO under scenarios with mobility and seek coverage enhancement solutions.

The rest of the paper is organized as follows. Section II describes how to optimize the baseband design of the 3D-MIMO, e.g. multiuser pairing and traffic adaptation. Section III analyzes the hardware design of 3D-MIMO where practical implementation constraints are considered, and tradeoff among cost, weight, size, heat dissipation of the product and its performance are made. Section IV describes the field trials of 3D-MIMO. Section V summarizes the 3D-MIMO design and hardware optimization, and concludes the field trial results.

II. Baseband Design for 5G 3D-MIMO System

In this section, the baseband design of 3D-MIMO for time-division duplex (TDD) transmission is elaborated, where tradeoffs are made between practical benefits and implementation constraints.

A. Model for Antenna Array and Transceivers

A two dimensional planar uniformly spaced antenna array is considered, as illustrated in Fig. 1. Denote the total number of antenna elements in the antenna array as N_{T}, and denote the structure of the array as (N_{V}, N_{H}, N_{P}), where N_{H} is the number of columns for antenna elements, N_{V} is the number of

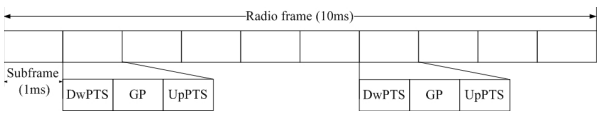

Fig. 2. Frame structure considered in 3D-MIMO system, where the DwPTS represents downlink pilot time slot, UpPTS represents uplink pilot time slot and GP represents guard period for downlink and uplink switching.

antenna elements with the same polarization in each column, and N_{P} is the number of polarization dimensions. Then $N_T = N_{\mathrm{V}} N_{\mathrm{H}} N_{\mathrm{P}}$. In this paper, co-polarized antenna elements are considered, which means $N_{\mathrm{P}} = 2$. The spacing between two adjacent antenna elements in vertical and horizontal domains are denoted as d_{V} and d_{H}.

Considering the importance of channel reciprocity of TDD for 3D-MIMO, the antenna element calibration is well designed and deployed inside the product, where calibration is performed periodically every few hours. The phase difference among antenna elements after calibration can be less than five degrees, which helps to improve the performance of 3D-MIMO transmission.

Denote the total number of radio frequency (RF) transceivers as N_{RF}. Similar as the description of antenna array, the structure of RF transceivers is represented as $(N_{\mathrm{V}}^{\mathrm{RF}}, N_{\mathrm{H}}^{\mathrm{RF}}, N_{\mathrm{P}}^{\mathrm{RF}})$, where $N_{\mathrm{H}}^{\mathrm{RF}}$ is the number of columns for RF transceivers, $N_{\mathrm{V}}^{\mathrm{RF}}$ is the number of RF transceivers with the same polarization in each column, and $N_{\mathrm{P}}^{\mathrm{RF}}$ is the number of polarization dimensions. Then $N_{\mathrm{RF}} = N_{\mathrm{V}}^{\mathrm{RF}} N_{\mathrm{H}}^{\mathrm{RF}} N_{\mathrm{P}}^{\mathrm{RF}}$. Although the RF transceivers do not needs to be with the same placement as that of antenna array, such description help for description for the connection from antenna array to the RF transceivers.

B. Physical Layer Design

1) Basic Transmission Assumptions: Since standardization of 5G is still on going, we reuse the frame structure, physical channel and reference signal design of LTE for the considered 3D-MIMO system. Such design can leverage the commercial LTE network for the field trial of 3D-MIMO, i.e., the commercial LTE devices can be applied and the practical inter-cell interference can be generated by the LTE Evolved Node B (eNB) to the targeted 3D-MIMO system.

The downlink waveform is orthogonal frequency-division multiplexing (OFDM) and the uplink wave-form is Single-carrier Frequency-Division Multiple Access (SC-FDMA). The LTE frame structure type 2 is considered [20], as shown in Fig. 2. The subcarrier spacing is 15kHz. The physical resource block (PRB) constitute the minimum time-frequency granularity, which consists of 12 subcarriers in frequency domain and single subframe in time domain.

The LTE cell-specific reference signal (CRS) is transmitted for reference signal receive power (RSRP) measurement, and demodulation of both broadcast signal and downlink control signal. The LTE demodulation reference signal (DMRS) design is reused, and the precoding of the DMRS is the same as the downlink data, so as to assist the channel estimation for downlink data demodulation. The maximum number of precoded layers for DMRS is two (antenna ports 7 and 8 in LTE Rel-10 specification [20]). If more than 2 UEs are multiplexed, the DMRS are multiplexed using the space division multiple access (SDMA) scheme. The uplink sounding reference signal (SRS) is transmitted for eNB to acquire channel state information (CSI) based on channel reciprocity.

2) Signal Model: Denote the number of subcarriers by K and the number of resolvable paths of channel impulse response (CIR) by L. Assuming that on each subcarrier, maximum of M users (UE) can be multiplexed, where each UE is equipped with N_r antennas and total S data streams are transmitted to each UE. In the following, we will omit the index of subcarrier for brevity.

Denote the channel vector between the N_r antennas at UE_m the (n_h, p, n_v)-th antenna element in the antenna array of base station as $\boldsymbol{h}_{m,n_h,n_v,p}^{\mathrm{A}} \in \mathbb{C}^{N_r \times 1}$, where $n_h = 1, \ldots, N_{\mathrm{H}}$, $n_v = 1, \ldots, N_{\mathrm{V}}$, $p = 1, \ldots, N_{\mathrm{P}}$. The channel between the UE_m and the n_h-th column with the pth polarization of the antenna array at base station can be denoted as $\boldsymbol{H}_{m,n_h,p}^{\mathrm{A}} = [\boldsymbol{h}_{m,n_h,1,p}^{\mathrm{A}}, \ldots, \boldsymbol{h}_{m,n_h,N_{\mathrm{V}},p}^{\mathrm{A}}] \in \mathbb{C}^{N_r \times N_{\mathrm{V}}}$, where $n_h = 1, \ldots, N_{\mathrm{H}}$. Consider cross-polarized antenna array, then $N_{\mathrm{P}} = 2$. The channel between the UE_m and all the antenna elements of the base station can be represented as $\boldsymbol{H}_m^{\mathrm{A}} = [\boldsymbol{H}_{m,1,1}^{\mathrm{A}}, \boldsymbol{H}_{m,1,2}^{\mathrm{A}}, \ldots, \boldsymbol{H}_{m,N_{\mathrm{H}},1}^{\mathrm{A}}, \boldsymbol{H}_{m,N_{\mathrm{H}},2}^{\mathrm{A}}] \in \mathbb{C}^{N_r \times N_{\mathrm{T}}}$.

Then the received signal of UE_m is

$$\boldsymbol{y}_m = \sum_{l=1}^{M} \boldsymbol{H}_m^{\mathrm{A}} \boldsymbol{W}_l \boldsymbol{s}_l + \mathtt{Inf}_m + \boldsymbol{z}_m, \tag{1}$$

where $\boldsymbol{W}_l \in \mathbb{C}^{N_{\mathrm{T}} \times S}$ is the precoding matrix for the data transmission to UE_l, $\boldsymbol{s}_l$ is data intended for UE_l, the term $\mathtt{Inf}_m$ represents the inter-cell interference received by UE_m. $\boldsymbol{z}_m$ is the Additive White Gaussian Noise (AWGN) with zero mean and covariance σ_z^2.

3) Precoding: Denote the baseband digital precoder as $\boldsymbol{W}_m^{\mathrm{BB}} \in \mathbb{C}^{N_{\mathrm{RF}} \times S}$, which processes S data streams to produce N_{RF} RF outputs. Then the basband signal are upconverted to RF signals and mapped to N_{T} antenna elements for transmission via an analog precoder $\boldsymbol{W}_m^{\mathrm{RF}} \in \mathbb{C}^{N_{\mathrm{T}} \times N_{\mathrm{RF}}}$. The precoder for UE_m is $\boldsymbol{W}_m = \boldsymbol{W}_m^{\mathrm{RF}} \boldsymbol{W}_m^{\mathrm{BB}}$. The digital and analog hybrid precoder can be jointly optimized to achieve optimal performance, which involves unaffordable complexity in practical application [21]. Decoupled sub-optimal design needs to be considered for ease of implementation in practical product.

The hybrid precoder considered herein is based on sub-array mapping from one transceiver to a number of antenna elements in vertical domain of the antenna array, as shown in Fig. 3. The N_{V} antenna elements in one column is divided into $N_{\mathrm{V}}^{\mathrm{RF}}$ groups, where each group consists of $K = N_{\mathrm{V}}/N_{\mathrm{V}}^{\mathrm{RF}}$ adjacent antenna elements. No analog precoder is applied for the horizontal domain of the antenna array, i.e., $N_{\mathrm{H}} = N_{\mathrm{H}}^{\mathrm{RF}}$ and $N_{\mathrm{P}}^{\mathrm{RF}} = N_{\mathrm{P}}$, since it has been verified by simulations in [19] that placing more RF transceivers for antenna elements in horizontal domain provides more performance gain. The precoder applied for connecting K antenna elements to a RF transceivers is denoted as $\boldsymbol{w}_{\mathrm{V}} \triangleq [w_1, ..., w_K]^T$. To ensure good coverage while reduce inter-cell interference, the analog

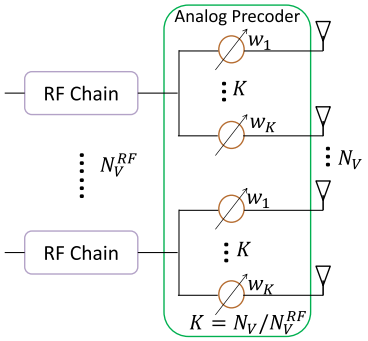

Fig. 3. Mapping from N_{V} antenna elements in one column of the antenna array with the same polarization to $N_{\mathrm{V}}^{\mathrm{RF}}$ RF transceivers.

precoder considered in this paper is fixed precoder as $w_k = \frac{1}{K} exp\{-j\frac{2\pi}{\lambda}(k-1)d_V \cos\theta_{\mathrm{vtilt}}\}$, $k = 1, \ldots, K$, where λ is the wave length and θ_{vtilt} is the down tilt direction.[1] Based on the above design, the analog precoder can be constructed by the block digitalization of N_{RF} vectors of $\boldsymbol{w}_{\mathrm{V}}$,

$$\boldsymbol{W}_m^{\mathrm{RF}} = \begin{pmatrix} \boldsymbol{w}_{\mathrm{V}} & \mathbf{0} & \cdots & \mathbf{0} \\ \mathbf{0} & \boldsymbol{w}_{\mathrm{V}} & \cdots & \mathbf{0} \\ \vdots & \vdots & \ddots & \\ quad vdots & & & \\ \mathbf{0} & \mathbf{0} & \cdots & \boldsymbol{w}_{\mathrm{V}} \end{pmatrix}. \tag{2}$$

where $\mathbf{0}$ is a vector of size $K \times 1$ with all elements as zero.

To simplify the notation for digital precoder, further define the channel between the UE$_m$ and the transceivers of the base station as $\boldsymbol{H}_m \triangleq \boldsymbol{H}_m^{\mathrm{A}} \boldsymbol{W}_m^{\mathrm{RF}}$.

The digital precoders for both SU-MIMO and MU-MIMO transmission are considered. For the SU-MIMO, the precoder design is based on eigen-beamforming [22] and equal power allocation. For the MU-MIMO, Block diagonalized Zero-forming (ZFBD) [23] is applied.

For the SU-MIMO transmission, denote the estimation of $\boldsymbol{H}_m$ at BS by $\hat{\boldsymbol{H}}_m$. The SVD decomposition of $\hat{\boldsymbol{H}}_m$ can be expressed as

$$\hat{\boldsymbol{H}}_m = \boldsymbol{U}_m \boldsymbol{\Lambda}_m \boldsymbol{V}_m^H, \tag{3}$$

where $\boldsymbol{U}_m \in \mathbb{C}^{N_r \times N_r}$, $\boldsymbol{\Lambda}_m \in \mathbb{C}^{N_r \times N_{\mathrm{RF}}}$ and $\boldsymbol{V}_m \in \mathbb{C}^{N_{\mathrm{RF}} \times N_{\mathrm{RF}}}$. The baseband precoder $\boldsymbol{W}_m^{\mathrm{BB}}$ in (1) is the first S columns of $\boldsymbol{V}_m$, i.e., $\boldsymbol{W}_m^{\mathrm{BB}} = \boldsymbol{V}_m(:, 1:S)$ [24].

For the MU-MIMO transmission with ZFBD precoder, denote the estimated composed channel matrices of all UEs except UE$_m$ by

$$\overline{\boldsymbol{H}}_m = [\hat{\boldsymbol{H}}_1^T, \ldots, \hat{\boldsymbol{H}}_{m-1}^T, \hat{\boldsymbol{H}}_{m+1}^T, \ldots, \hat{\boldsymbol{H}}_M^T]^T, \tag{4}$$

where $\overline{\boldsymbol{H}}_m \in \mathbb{C}^{(M-1)N_r \times N_{\mathrm{RF}}}$.

Let the $R_m = \mathrm{rank}(\overline{\boldsymbol{H}}_m)$. The SVD decomposition of $\overline{\boldsymbol{H}}_m$ is $\overline{\boldsymbol{H}}_m = \overline{\boldsymbol{U}}_m \overline{\boldsymbol{\Lambda}}_m [\overline{\boldsymbol{V}}_m^{(1)} \overline{\boldsymbol{V}}_m^{(0)}]^H$, where $\overline{\boldsymbol{V}}_m^{(1)}$ holds the first R_m right singular vectors, and $\overline{\boldsymbol{V}}_m^{(0)}$ holds the last $(N_{\mathrm{RF}} - R_m)$ right singular vectors. Thus, $\overline{\boldsymbol{V}}_m^{(0)}$ forms an orthogonal basis for the null space of $\overline{\boldsymbol{H}}_m$.

The projection of channel of UE$_m$ on the null space of $\overline{\boldsymbol{H}}_m$ can be denoted by $\hat{\boldsymbol{H}}_1 \overline{\boldsymbol{V}}_m^{(0)}$, and its rank is $\widetilde{R}_m = \mathrm{rank}(\hat{\boldsymbol{H}}_1 \overline{\boldsymbol{V}}_m^{(0)})$. The SVD decomposition of the projected channel matrix can be expressed as

$$\hat{\boldsymbol{H}}_1 \overline{\boldsymbol{V}}_m^{(0)} = \widetilde{\boldsymbol{U}}_m \widetilde{\boldsymbol{\Lambda}}_m [\widetilde{\boldsymbol{V}}_m^{(1)} \widetilde{\boldsymbol{V}}_m^{(0)}]^H, \tag{5}$$

where $\widetilde{\boldsymbol{V}}_m^{(1)}$ represents the first $\widetilde{R}_m$ right singular vectors, and $\widetilde{\boldsymbol{V}}_m^{(0)}$ represents the last $(N_{\mathrm{RF}} - \widetilde{R}_m)$ right singular vectors.

The product of $\overline{\boldsymbol{V}}_m^{(0)}$ and $\widetilde{\boldsymbol{V}}_m^{(1)}$ produces an orthogonal basis of dimension $\widetilde{R}_m$ and represents the transmission vectors that maximize the data rate for user subject to produce zero interference. Then the beamforming matrix $\boldsymbol{W}_m^{\mathrm{BB}}$ can be denoted by

$$\boldsymbol{W}_m^{\mathrm{BB}} = \overline{\boldsymbol{V}}_m^{(0)} \widetilde{\boldsymbol{V}}_m^{(1)}. \tag{6}$$

4) Scheduling: For frequency domain scheduling, the well-known Proportional Fair (PF) algorithm [25] is considered. When the scheduling granularity in frequency domain is one key component that influence the performance, i.e., the smaller of the granularity, the best performance can be achieved while with higher complexity. To achieve a tradeoff between performance and the complexity, the frequency domain scheduling granularity is determined as follows. For the scheduling of the nth subframe, the eNB calculate the required number of PRBs for transmission of each UE based on the assumption of SU-MIMO transmission, which is determined as the minimum scheduling granularity.

For the MU-MIMO scheduling, to exploit the spacial multi-user diversity while keeping low complexity, the semi-orthogonal user scheduling in [26] is applied, where the instantaneous channel state information (CSI) is replaced by the eigenvector of channel covariance matrix in the considered frequency granularity.

5) Receivers at UEs: The receiver at UEs considered herein is minimum mean square error (MMSE) receiver. Define equivalent channel matrix after precoding of all the M multiplexed UEs as $\tilde{\boldsymbol{H}}_l \triangleq \boldsymbol{H}_m \boldsymbol{W}_l$, $l = 1, \ldots, M$. Assume that UE$_m$ can estimate $\tilde{\boldsymbol{H}}_{l,n}$, $l = 1, \ldots, M$, while only knows the interference power from other interfering base stations. Then the receiver of UE$_m$ can be represented as

$$\boldsymbol{U}_m = \hat{\tilde{\boldsymbol{H}}}_m^H \left(\sum_{l=1}^{M} \hat{\tilde{\boldsymbol{H}}}_l \hat{\tilde{\boldsymbol{H}}}_l^H + \sigma_{\mathrm{I}_m}^2 \right)^{-1}, \tag{8}$$

where $\hat{\tilde{\boldsymbol{H}}}_l$ is the estimation of $\tilde{\boldsymbol{H}}_l$ at UE$_m$, and $\sigma_{\mathrm{I}_{m,n}}^2$ is the estimation of noise plus interference power from other interfering base stations, i.e., the estimation of $(\mathrm{tr}\{\mathtt{Inf}_{m,n} \mathtt{Inf}_{m,n}^H\} + \sigma_z^2)$.

With the receiver, the data rate of the UE$_m$ can be represented by equation (7), shown at the bottom of the next page.

III. Hardware Design for 5G 3D-MIMO Trial System

In this section, the factors of the practical 3D-MIMO hardware design will be discussed and the corresponding tradeoffs between performance and implementation constraints will be

[1] Although the analog precoder can be adjusted dynamically, it is not considered in this paper, since dynamic analog precoding will involve more complicated initial access and control channel design based on the analog beamforming, which are now still under standardization of 3GPP for 5G.

TABLE I
COMPARISON OF ANTENNA SIZE AND WEIGHT FOR 3D-MIMO AND COMMERCIAL LTE TDD ANTENNA, WHERE THE RRU REPRESENTS THE REMOTE RADIO UNIT

	Commercial LTE TDD antenna	5G 3D-MIMO with 128 antenna elements
windward	0.14 m^2 RRU + 0.45m^2 antenna panel	0.45m^2
weight	21kg RRU + 11kg antenna panel	45kg

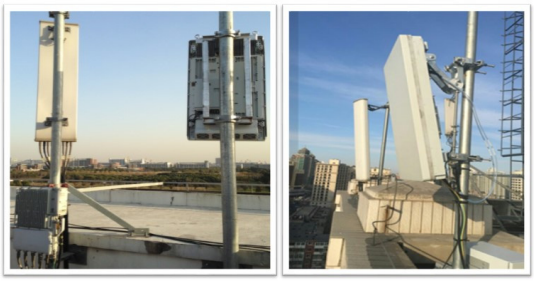

Fig. 4. Comparison of antenna size for 3D-MIMO with 128 antenna elements and commercial LTE TDD antenna, where in each sub-figure the left one is LTE TDD antenna and the right one is the 3D-MIMO.

investigated in detail. The 2.6GHz TDD frequency band is considered.

A. Antenna Array Design

The antenna array size for commercial deployment is limited by wind load and feasibility of installation on the tower. In order to meet the wind load requirement in typical urban scenario, the antenna array size of a base station should not exceed 6000 cm^2. Aiming for feasibility of installation on the tower, the antenna array size of the vertical domain should be larger than that of horizontal domain. Since the larger the antenna array size is, the better of the heat dissipation performance in addition to the throughput performance, the antenna array size is chosen to be less than or equal to 6000 cm^2.

Based on the given antenna array size, the number of antenna elements in the array depends on spacing between adjacent antenna elements. Usually, half-wavelength is selected as typical spacing for two adjacent antenna elements in horizontal direction, i.e., $d_{\mathrm{H}} = 0.5\lambda$, and 0.7 wavelength is chosen as that in vertical direction, i.e., $d_{\mathrm{V}} = 0.7\lambda$. Since the design is for 2.6GHz, the wavelength is $\lambda = 11.5$cm. Then $d_{\mathrm{H}} = 0.5\lambda = 5.75$cm and $d_{\mathrm{V}} = 0.7\lambda = 8.05$cm. To fit into a planar antenna array with size around 6000 cm^2 while with the antenna array size of the vertical domain be larger than that of horizontal domain, one feasible antenna array structure is $(N_{\mathrm{V}}, N_{\mathrm{H}}, N_{\mathrm{P}}) = (8, 8, 2)$, which means total of $N_{\mathrm{T}} = 128$ antenna elements can be accommodated. A comparison of antenna array size for such 3D-MIMO and commercial LTE TDD antenna is shown in Fig. 4, where the structure of LTE TDD antenna array is $(N_{\mathrm{V}}, N_{\mathrm{H}}, N_{\mathrm{P}}) = (8, 4, 2)$. The comparison on wind load area and weight for 3D-MIMO and LTE TDD antenna are provided in Table I.

B. Tradeoff on Number of RF Transceivers

Theoretically, the one-to-one mapping from RF transceivers to antenna elements with full digital precoding capability can achieve the best performance. However, 3D-MIMO product with $N_{\mathrm{RF}} = N_{\mathrm{T}} = 128$ RF transceivers is less attractive commercial-wise, in terms of cost, weight, size and heat dissipation.

With the increase of the RF transceivers, the cost, weight and size of the 3D-MIMO product needs to be increased accordingly. As for the power efficiency, typically, it degrades with the decrease of the output power of power amplifier (PA). For example, for the existing LTE TDD macro eNB with 8 transceivers, the power efficiency for each transceiver is around 40% for the PA output power of around 15Watt, which indicates that around 100Watt power consumption is required with output power of 40Watt, which is the typical requirement of effective isotropic radiation power for the LTE TDD antenna. As for 2.6GHz 3D-MIMO, the power efficiency of available PA with output power less than 1 Watt is around 10%. To achieve the same effective isotropic radiation power as the LTE TDD antenna, more than 400Watt power consumption is required by the RF transceivers. Such low power efficiency leads a big risk for heat dissipation of the whole radio unit.

Tradeoff need to be considered in the 3D-MIMO product between performance enhancement and the above mentioned implementation issues brought be increasing the RF transceivers. To verify the impact of number of RF transceivers on 3D-MIMO performance, system-level simulation is done to compare the performance of four possible structures of RF transceivers. The four structures in terms of $(N_{\mathrm{V}}^{\mathrm{RF}}, N_{\mathrm{H}}^{\mathrm{RF}}, N_{\mathrm{P}}^{\mathrm{RF}})$ are $(1, 8, 2)$, $(2, 8, 2)$, $(4, 8, 2)$ and $(8, 8, 2)$. For these four structures, the total number of RF transceivers N_{RF} are 16, 32, 64 and 128, respectively.

1) System-Level Simulation Setup: We consider a 7 cell sites deployment with inter-site distance as 500m and 3 sectors per site. A cell site is located in the center for simulation of the

$$R_m = \log_2 \det \left\{ \boldsymbol{I} + \left(\sigma^2_{\mathrm{I}_m} \boldsymbol{U}_m \boldsymbol{U}_m^H + \boldsymbol{U}_m \sum_{l=1, l\neq m}^{M} \boldsymbol{H}_m^{\mathrm{A}} \boldsymbol{W}_l \boldsymbol{W}_l^H (\boldsymbol{H}_m^{\mathrm{A}})^H \boldsymbol{U}_m^H \right)^{-1} \boldsymbol{U}_m \boldsymbol{H}_m^{\mathrm{A}} \boldsymbol{W}_m \boldsymbol{W}_m^H (\boldsymbol{H}_m^{\mathrm{A}})^H \boldsymbol{U}_m^H \right\} \tag{7}$$

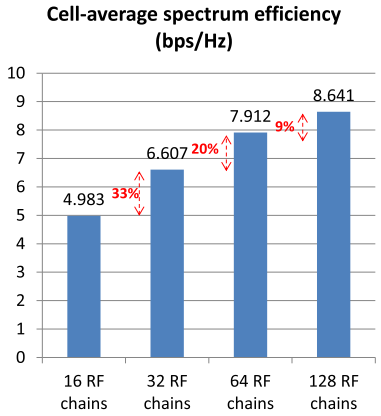

Fig. 5. Performance comparison of different architectures of RF transceivers.

performance and the other 6 cell sites are located around the targeting cell to perform as interference. The bandwidth is 20MHz on 2.6GHz TDD band. The UEs are equipped with two isotropic antennas that are co-located with cross polarization. The speed of UEs are 3km/h. The number of UEs in each sector is 10. Full buffer traffic is considered and the 3D channel model that are approved in 3GPP [27] is applied. MU-MIMO transmission is considered with maximum number of spatial multiplexed UEs as 8.

The CSI for precoding is obtained by channel reciprocity. The channel quality information for adaptation of modulation and coding scheme are feedback by UE every 5ms. To simulate real channel estimation error while reduce simulation complexity, the uplink channel estimation error is modeled as $\hat{h} = \alpha(h + e)$, where α is the scaling factor to maintain norm normalization of estimated channel, h is the small scale fading channel and e is white complex Gaussian variable with zero mean and variance σ_e^2 that incorporates the channel estimation error. The variance σ_e^2 is given as $\sigma_e^2 = 1/(\mathrm{SINR} + \Delta)$, where SINR represents the received SINR of uplink training sequences at the BS, and Δ is the gain obtained from time domain filtering during channel estimation. The scaling factor is given as $\alpha = \sqrt{\frac{1}{1+\sigma_e^2}} = \sqrt{\frac{\Delta * \mathrm{SINR}}{\Delta * \mathrm{SINR}+1}}$, and the $\Delta = 9$ dB.

2) Simulation Results: In Fig. 5 the cell-average spectral efficiency of different RF transceiver structures are provided. The cell-average is the average of the spectrum efficiency of the cell, which is obtained as

$$\mathrm{SE} = M_{\mathrm{DL}} \frac{1}{N * \mathrm{BW}} \sum_{n=1}^{N} \sum_{k=1}^{N_K} \sum_{m=1}^{M} R_m(n,k), \tag{9}$$

where N_K is the number of subcarriers considered in the system, BW is the bandwidth of the system, N is the number of downlink subframes in the simulation, M_{DL} is the number of downlink subframes in one second, and since TDD DL and UL configuration 2 in LTE is applied, then $M_{\mathrm{DL}} = 600$. $R_m(n,k)$ is the data rate of the UE_m at the kth subcarrier of the nth subframe, and the value of $R_m(n,k)$ is derived based on equation (7).

It can be seen that although the performance of 3D-MIMO increases as more transceivers are introduced in the system, while the extra performance gain by more transceiver diminishes. With 32 transceivers, the performance gain over 16 transceivers is 33%. By contrast, the performance gain of 64 transceivers over 32 transceivers reduces to 20%. If 128 RF transceivers are applied, the performance can be only enhanced by 9% compared with the performance of 64 transceivers.

The more transceivers provide more spatial freedom for beamforming and multiuser multiplexing, which leads to higher performance gain. But such gain cannot be increased approximately to the transceiver number. On one hand, due to the very narrow beam sweeping scope in vertical domain compared to the horizontal domain, the more spatial freedom in vertical domain contribute less extra performance gain than that of horizontal domain. On the other hand, the performance gain of MU-MIMO is limited by the number of spatial multiplexed UEs. When maximum number of spatial multiplexed UEs is limited and much more transceivers are introduced, the benefits of increasing transceivers are enhancing the signal-to-noise ratio (SNR) for each UE, whose contribution to the date rate is in logarithmic scale. In practical network deployment, it is difficult to find more than 16 users to be multiplexed simultaneously.

According to the performance results and implemental limitations, the 64 transceivers structure can achieve a good balance are implemented in product for performance validation in field trials.

C. Hardware Architecture Design

The traditional LTE base station deployed in commercial networks is composed of baseband unit (BBU), remote radio unit (RRU) and passive antennas, as shown in Fig. 6. The passive antennas are installed on the top of a tower and connected to the RRU by cables, while the RRU is connected to the BBU by fibers. To enable more freedom in spatial domain, 3D-MIMO with massive antennas requires more transceivers to be integrated in the eNB. If the traditional architecture with distributed BBU, RRU and antennas are kept, more cables and fibers are required to connect the BBU, RRU and antennas, which not only increases the cost but also introduces cable loss. In addition, ports of antenna array need to be manually connected to RRU, adding a significant burden for antenna installation. Integrating the active transceivers and the passive antenna array into one unit helps avoid cable connections between antennas and RRU, and mitigate the cable loss. Such integrated unit is termed as active antenna system (AAS), which is considered to be a promising structure for future 5G systems.

Whether to integrate BBU and AAS in the same unit is another issue that needs to be addressed for the commercial deployment of 3D-MIMO with massive antennas. Integrating of BBU and AAS into a single unit, as illustrated in Fig. 6, helps reduce the cost of fibers and corresponding connecting units, making the sites cleaner. However, the size of the integrated unit might be too large for commercial deployment and the weight might become a severe problem for installation. In addition, the heat dissipation issue of such integrated set

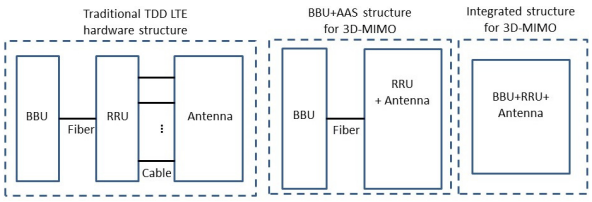

Fig. 6. Hardware architecture comparison of 5G 3D-MIMO and traditional LTE TDD systems.

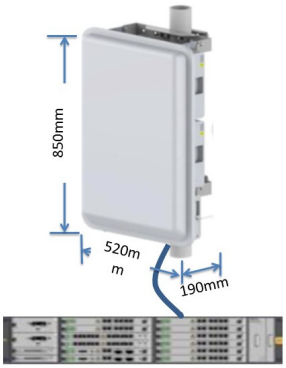

Fig. 7. A 3D-MIMO product for 5G, with 128 antenna elements and 64 RF transceivers aggregated in AAS and being connected to BBU by fiber.

is quite difficult to solve, due to the limited area for heat dissipation. Another defect of this integrated architecture is that baseband software upgrade will become quite difficult. Moreover, the baseband unit processing capability upgrade, which is usually done by replacing the hardware after deployment, also becomes infeasible, since the whole integrated unit is installed on the top of tower. On the other hand, the non-integrated architecture where AAS is connected to BBU on the ground by fibers, as illustrated in Fig. 6, is more promising since the weight and ungrade issues mentioned above can be avoided, even though fibers with high capacity are required for this architecture. For a system with 60 MHz bandwidth, the capacity of the fiber should be no less than 240 Gbps if no data compression is applied. The requirement can be lowered to 100 Gbps if data compression with 1/3 to 1/2 compression rate is applied. In practice, such requirement can be met by using one fiber with 100 Gbps capacity, or using 4 fibers, each with 25Gbps capacity. Based on the above analysis, a promising 3D-MIMO product design for 5G is proposed and illustrated in Fig. 7, where 128 antenna elements and 64 RF transceivers aggregated in AAS and being connected to BBU by fiber.

IV. Field Trial of 5G 3D-MIMO in Typical Scenarios

In this section, two field trials are conducted to verify the performance of 3D-MIMO. The first trial aims to test the maximum capability of the 3D-MIMO and to performance comparison of field trial and simulation. Hence, full buffer traffic model is adopted. The second trial aims to evaluate the performance of 3D-MIMO in real network. Therefore, commercial UEs and real network traffic are used. In the trial,

Fig. 8. Test scenario for fixed location UEs, with the location of all UEs far away to each other. (Note that locations within each circle indicate that those users are distributed in different storeys in the building.)

UEs with 2 receiving antennas and single transmitting antenna are used.

The main difference of the trial in this paper compared with those in [16]–[19] is that the 3D-MIMO system is deployed in a commercial network where the LTE sites are operating at the same frequency band. Therefore, the impact of inter-cell interference in practical systems are considered. The carrier frequency used in the test is 2575-2595 MHz with 20 MHz bandwidth. To avoid introducing additional uplink-downlink interference, the frame structure of the 5G system aligns with that of the commercial LTE network, where the LTE uplink-downlink configuration 2 is adopted [20]. In this configuration, three downlink subframes, single uplink subframe and single special subframe with both downlink and uplink are allocated within a period of 5 ms.

To fairly compare the performance of 5G 3D-MIMO and that of current LTE TDD system, the 3D-MIMO base stations are co-sited with LTE based stations. For LTE TDD system, the SU-MIMO is enabled. To maximize the LTE performance, the adaptation of dual-layers and single-layer transmission is applied based on instantaneous CSI from channel reciprocity. The downtilts of 3D-MIMO base stations are optimized independently, without affecting the existing LTE network. For both the simulation and the field trial, the antenna array structure and RF transceivers for LTE TDD are $(N_{\mathrm{V}}, N_{\mathrm{H}}, N_{\mathrm{P}}) = (8, 4, 2)$, and $(N_{\mathrm{V}}^{\mathrm{RF}}, N_{\mathrm{H}}^{\mathrm{RF}}, N_{\mathrm{P}}^{\mathrm{RF}}) = (1, 4, 2)$. The antenna array structure and RF transceivers for 3D-MIMO are $(N_{\mathrm{V}}, N_{\mathrm{H}}, N_{\mathrm{P}}) = (8, 8, 2)$, and $(N_{\mathrm{V}}^{\mathrm{RF}}, N_{\mathrm{H}}^{\mathrm{RF}}, N_{\mathrm{P}}^{\mathrm{RF}}) = (4, 8, 2)$.

A. Field Trial of 5G 3D-MIMO With Full Buffer Traffic

To test the maximal spectral efficiency gain achieved by 3D-MIMO, UEs with stationary locations are applied. To evaluate the impact of the number of multiplexed UEs on the performance gain, the maximum number of multiplexed UEs for MU-MIMO transmission are set to be 16 and 8, respectively. Two types of UEs' locations are considered. Case1: 16 UEs are uniformly distributed in a given area, as illustrated in Fig. 8. Case2: 16 UEs are divided into groups and UEs in each group are closely located, as shown in Fig. 9.

TABLE II
BENEFITS AND CHALLENGES OF TWO BS ARCHITECTURES WITH DIFFERENT LEVEL OF INTEGRATIONS

Architectures	**Benefits**	**Challenges**
BBU+AAS	Low weight of site, convenient future upgrade of baseband	High capacity requirements of fiber
Single unit with BBU and AAS	No fiber, cleaner sites	Stringent requirements on the size, weight and heat dissipation

TABLE III
CELL THROUGHPUT COMPARISON FOR LTE TDD AND 3D-MIMO

	LTE TDD	5G 3D-MIMO	Performance gain
Field Trial Max16UEs	44.1Mbps	341.3Mbps	773%
Field Trial Max8UEs	44.1Mbps	209Mbps	475%
Simulation Results Max8UEs	32.4Mbps	118.7Mbps	366%

Fig. 9. Test scenario for fixed location UEs, with four groups of UEs and the UEs in each group near to each other. (16 users are divided into four groups. The distance among groups is relatively far while the distance among users within the same group is less than 1 meter. The users are distributed in the locations marked in red.)

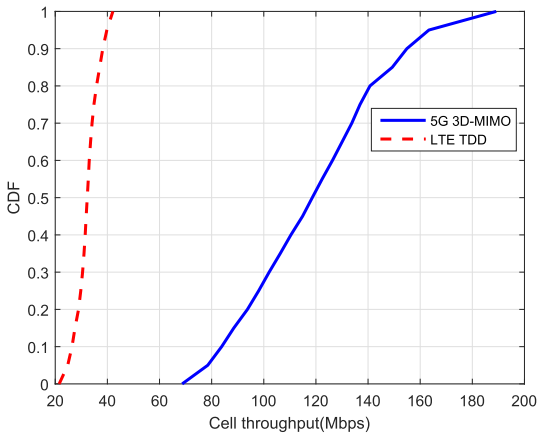

Fig. 10. CDF of cell throughputs for LTE and 3D-MIMO obtained by system-level simulation.

The average cell throughput are provided for performance comparison, which is defined as $\overline{R}_{\text{cell}} \triangleq M_{\text{DL}} \frac{1}{N} \sum_{n=1}^{N} R_{\text{cell}}(n)$, where $R_{\text{cell}}(n)$ is the instantaneous cell throughput at the nth subframe, N is the number of downlink subframes in the tested period, M_{DL} is the number of downlink subframes in one second. Since TDD DL and UL configuration 2 in LTE is applied, then $M_{\text{DL}} = 600$.

1) Performance Comparison of Field Trial and Simulation: To verify the performance of 3D-MIMO over LTE, system-level simulation is done based on the simulation assumption described in Section III.B.2). The CDF curves for the average cell throughput of 3D-MIMO over LTE are illustrated in Fig. 10, where the different samples in the CDF curve are obtained under different snapshots of randomly distributed UEs. By careful planning of the base stations and fair scheduling, multiple users are scheduled simultaneously in frequency domain and spatial domain of one subframe, so the cell throughput will not be 0 anytime. The performance of the 3D-MIMO is much better than that of LTE system.

The average cell throughputs obtained from both system-level simulation and field trial are provided in Table III, where the "Max16UEs" and "Max8UEs" represent cases where the maximum numbers of multiplexed UEs are 16 and 8, respectively. In this field trial, the UEs' locations described in Case1 is considered.

Comparing the simulation and the field trial results, it is observed that the throughput and the performance gain of field trial are better than that of system-level simulations. There are two main reasons behind this observation. First, the inter-cell interference in field trial is expected to be less than that in the system-level simulation, since the inter-cell interference in field trial is caused by commercial LTE eNB with very light traffic load, while full buffer traffic is considered in the simulation. Second, the UE channel conditions are slightly different in simulation and trials. For the field trial, 16 UEs with fixed locations are considered, while in simulation, the UEs are randomly located.

By comparing the field trial results for maximum 16 and 8 multiplexed UEs, it is observed that supporting higher order of MU-MIMO multiplexing transmission helps enhance the performance, and the performance gain is about 63.1%. It is worth noting that the throughput of 3D-MIMO with maximum of 16 and 8 multiplexed UEs are approximately 7.7 times and 4.7 times of that of LTE, meeting the 5G spectral

TABLE IV
CELL THROUGHPUT COMPARISON FOR UES WITH SOME UES ARE CLOSELY LOCATED

	LTE TDD	5G 3D-MIMO	Performance gain
Field Trial Max16UEs	35.27Mbps	173.97Mbps	493%
Field Trial Max8UEs	35.27Mbps	120.24Mbps	340%

Fig. 11. Test scenario for campus area. The left figure shows the deployed 3D-MIMO with massive antennas (abbreviated as MM in the figure) and the LTE TDD system (abbreviated as 8T in the figure). The right figure shows the coverage area for the scenario.

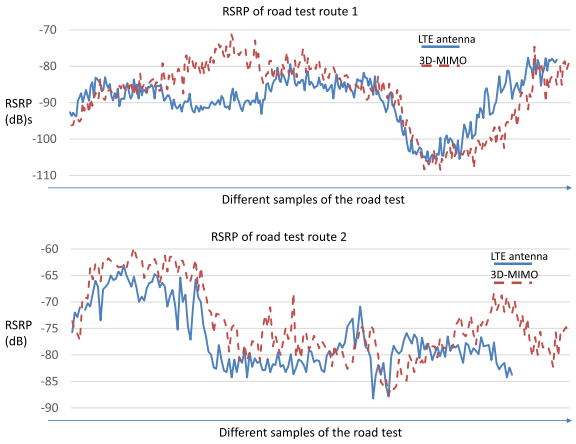

Fig. 12. RSRP performance of a road test UE for LTE TDD and 5G 3D-MIMO with massive antennas in campus scenario.

efficiency target. The reason why such significant improvement can be achieved is that the LTE system employs SU-MIMO transmission with maximum 2 layers per UE and the 3D-MIMO system can multiplex much more UEs to fully exploit the gain of MU-MIMO transmission. It is also observed that the performance gain of 3D-MIMO over legacy LTE antenna is not linearly increased with the maximum number of multiplexed UEs. The reason is that in the field trial, the number of UEs can be multiplexed for MU-MIMO transmission depends on the CSI of the UEs, and it is observed that the number of actually multiplexed UEs cannot reach its upper limit most of the time. In addition, when more UEs are multiplexed, the multi-user interference is introduced due to imperfect CSI for precoding.

2) Impact of UEs' Location on Performance: In order to evaluate the impact of UE locations on performance of 3D-MIMO, the test results for Case2 of UEs' locations are provided in Table IV. It can be observed that the throughput of 3D-MIMO BSs are approximately 4.9 and 3.4 times that of LTE system, when maximum number of multiplexed UEs are 16 and 8, respectively. Compared with the results in Table III, it is shown that the scenario with group UEs reduces the performance gains of 3D-MIMO. The intuition behind this is that, when the ZFBD precoding is considered, if UEs closely located are scheduled for MU-MIMO transmission, the probability of having orthogonal channels for different UEs is low, resulting lower data rates. Nonetheless, even under such non-ideal circumstance, 3D-MIMO still manages to achieve the 5G spectral efficiency target.

B. Field Trial of 3D-MIMO With Commercial Traffics

The field trial is also carried out with commercial traffic, aiming at testing how the 5G 3D-MIMO system performs in a commercial network with real traffic. Four typical scenarios are considered, 1) campus scenario to test coverage performance, 2) dense urban scenario to test the capability of serving different traffic and services with large amount of UEs, 3) hot spot scenario to test the capability of handling explosive increase of traffic volume, and 4) mobility scenario to test the impact of mobility on the performance.

Considering that the instant data rate per cell highly depends on number of UEs served by the cell and their transmission behavior, the performance evaluation metric used in the test is the number of bits per Hz, where only the number of scheduled PRBs are used to calculate the bandwidth in the denominator. The rationale behind this is to eliminate the impact of traffic load on the performance evaluation. Denote this performance metric as spectral efficiency (SE). Note that the SE is derived based the resources available for data transmission, i.e., the overhead of reference signals, control channel and other broadcast channel have been excluded.

The provided results are averaged over several hours to remove the volatility. The SU-MIMO and MU-MIMO are adaptive based on the traffic and CSI of each subframe, and the maximum number of UEs multiplexed for MU-MIMO transmission is 16.

1) Coverage Performance in Campus Area: The 3D-MIMO base station is installed on a tower of approximately 40 meters, covering the area of a campus as shown in Fig. 11. The UE in the test moves at 30 km/h for several hours. The RSRP obtained by two typical routes are illustrated in Fig. 12.

It is observed that RSRP of the 3D-MIMO system is higher than that of LTE on average, since the AAS structure of 3D-MIMO help saving the cable loss compared with LTE by around 1∼2 dB. Besides, compared with the LTE TDD with 64 antenna elements, the 3D-MIMO with 128 antenna elements can provide higher array gain and better beam pattern

TABLE V
PERFORMANCE COMPARISON IN TYPICAL URBAN SCENARIO WITH COMMERCIAL TRAFFICS

	LTE TDD	5G 3D-MIMO	Performance gain
Downlink SE	1.86bps/Hz	4.62bps/Hz	149%

TABLE VI
PERFORMANCE COMPARISON IN TYPICAL URBAN MACRO SCENARIO WITH REALISTIC MOBILITY

	LTE TDD	5G 3D-MIMO	Performance gain
Downlink SE	1.56bps/Hz	2.71bps/Hz	74%

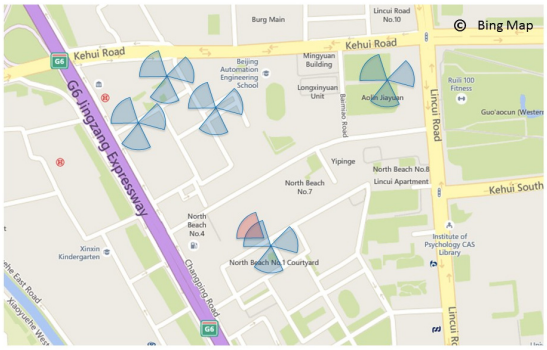

Fig. 13. Typical urban macros scenario for test of capacity, where the location of 3D-MIMO base station is marked in red, and the nearby interference LTE TDD systems are marked in blue.

Test point	RSRP (dBm)	SINR (dB)
l	-78.36	22.43
k	-75.86	21.3
b	-81.2	17.21
d	-83.68	12.76
g	-82.5	11.6
p	-89.76	10.62
n	-84.37	7.65
e	-89.89	6.64
c	-85.98	4.72
f	-84.03	3.87
j	-92.01	2.57
h	-102.66	1.98
i	-87.62	0.93
m	-81.9	0.89
o	-89.93	-0.91

Fig. 14. Typical dense urban macros scenario for test of capacity, with explosive large volume traffic. Besides the commercial UEs, maximum of 16 UEs with video traffics are added manually, as marked in the figure, with the corresponding RSRP and SINR listed at the right side of the figure.

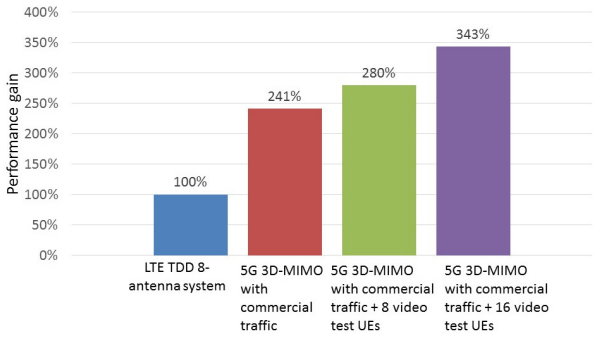

Fig. 15. Downlink performance enhancement of 3D-MIMO with massive antennas over LTE TDD systems with the increase of traffic volume.

for broadcasting. However, it is not always the case in some test locations. The reason behind this is that the RSRP is based on measurement of CRS where no UE-specific beamforming is performed. Therefore, in order to achieve better RSRP coverage than LTE, the reference signal and broadcast channel may also needed to be enhanced by adopting schemes that can reap the benefit of the multiple antennas, such as the beam sweeping solution.

2) Capacity Performance With Small-Packet Traffics: The test scenario is shown in Fig. 13, which is a typical dense urban macros scenario in commercial network. One typical traffic pattern in such scenario is that a large amount of UEs with small packets to communicate with the eNB simultaneously. The SE performance is shown in Table V. It is observed that the 3D-MIMO system under such scenario still can enhance the SE, and the performance gain over that of LTE is 149%. However, it is worth noting that the performance gain in this scenario with small-packet traffic is lower than that in the full-buffer test as shown in Table III. The reason behind this is that when the traffic is low and the UEs are with small-packet traffic, it is difficult for the base station to multiplex large number of UEs by MU-MIMO transmission, which degrades the performance gain of 3D-MIMO.

3) Validation on Impact of Traffic Load: In order to evaluate the performance of 3D-MIMO system in the 5G network where large traffic volume are expected, we choose a hot spot scenario as shown in Fig. 14, where a shopping mall is included. In addition to the commercial traffic in the LTE network, video-viewing UEs are added to the serving eNB, as shown in Fig. 14. In Fig. 15, the performance enhancement of 3D-MIMO over LTE TDD systems is provided. The results shown that the gain of the 5G 3D-MIMO over the legacy LTE network rises as the increase of traffic volume in the network. Therefore, 3D-MIMO with massive antennas can be considered as a crucial and efficient solution to cope with the heavy traffic load in future mobile network.

4) Mobility Performance: In order to evaluate the impact of mobility on performance of 3D-MIMO, tests are performed for UEs moving at pedestrian speed, 30 km/h and 60 km/h. The 3D-MIMO is located on a tower of approximately 60 meters,

Fig. 16. Typical mobility scenario, with the coverage area of the 3D-MIMO as shown in the figure. The test is performed during a traffic busy period, i.e., the vehicles are crowded and moves at relatively slow speed.

as illustrated in Fig. 16. The SE performance is shown in Table VI. Although the 3D-MIMO system still outperforms the LTE system, the performance gain decreases compared to those in scenarios where most of the UEs are with very low mobility as shown in Table V. The main reason of such performance degradation is that the performance of the 3D-MIMO system is highly sensitive to the timeliness and accuracy of CSI, which are impacted by medium or high mobility. These results highlight the necessity of further enhancement for 3D-MIMO with massive antennas in medium to high mobility scenarios.

V. Conclusions

In this paper, a systematic design for 3D-MIMO product design is proposed, where the tradeoff between performance and implementation limitations including cost, size, weight and heat dissipation are considered. A 5G 3D-MIMO structure with 128 antenna elements is designed and implemented at 2.6 GHz frequency band. Field trials of this 3D-MIMO design is performed with commercial LTE devices. The trial results show that 3D-MIMO can help 5G to achieve the spectral efficiency target which is 3 times of that of LTE. For full-buffer traffic, 4∼6.7 times cell throughput gains are observed for 3D-MIMO compared to the LTE TDD system with 8 antennas. For the field trial with the real commercial traffic, the performance gain of 3D-MIMO is lower than that in full-buffer test, while the performance gain increases when the traffic load is raised by adding more video-viewing users to the network. The field trial also shows that the coverage enhancement of 3D-MIMO over LTE is limited, bringing out the necessity on future 3D-MIMO enhancement on coverage. It is also shown that the mobility impacts the performance of 3D-MIMO and further enhancement on how to acquire timely and accurate CSI and measurement reports should be made to ensure that the performance of 3D-MIMO is robust in medium or high mobility scenarios.

References

[1] "White paper on 5G vision and requirements," Promotion Group, Beijing, China, Final Rep. IMT-2020 (5G), May 2014.

[2] "IMT vision- framework and overall objectives of the future development of IMT for 2020 and beyond," Int. Telecommun. Union, Geneva, Rep. M.2083-0, Sep. 2015.

[3] Y.-H. Nam *et al.*, "Full-dimension MIMO (FD-MIMO) for next generation cellular technology," *IEEE Commun. Mag.*, vol. 51, no. 6, pp. 172–179, Jun. 2013.

[4] R. W. Heath, N. González-Prelcic, S. Rangan, W. Roh, and A. M. Sayeed, "An overview of signal processing techniques for millimeter wave mimo systems," *IEEE J. Sel. Topics Signal Process.*, vol. 10, no. 3, pp. 436–453, Apr. 2016.

[5] T. L. Marzetta, "Noncooperative cellular wireless with unlimited numbers of base station antennas," *IEEE Trans. Wireless Commun.*, vol. 9, no. 11, pp. 3590–3600, Nov. 2010.

[6] J. Hoydis, S. T. Brink, and M. Debbah, "Massive MIMO in the UL/DL of cellular networks: How many antennas do we need?" *IEEE J. Sel. Areas Commun.*, vol. 31, no. 2, pp. 160–171, Feb. 2013.

[7] L. Lu, G. Y. Li, A. L. Swindlehurst, A. Ashikhmin, and R. Zhang, "An overview of massive MIMO: Benefits and challenges," *IEEE J. Sel. Topics Signal Process.*, vol. 8, no. 5, pp. 742–758, Oct. 2014.

[8] J. Zhang, C. Pan, F. Pei, G. Liu, and X. Cheng, "Three-dimensional fading channel models: A survey of elevation angle research," *IEEE Commun. Mag.*, vol. 52, no. 6, pp. 218–226, Jun. 2014.

[9] X. Lu, A. Tolli, O. Piirainen, M. Juntti, and W. Li, "Comparison of antenna arrays in a 3-D multiuser multicell network," in *Proc. IEEE ICC*, Jun. 2011, pp. 1–6.

[10] Y. Li, Y.-H. Nam, B. L. Ng, and J. Zhang, "A non-asymptotic throughput for massive mimo cellular uplink with pilot reuse," in *Proc. IEEE GLOBECOM*, Dec. 2012, pp. 4500–4504.

[11] B. L. Ng *et al.*, "Fulfilling the promise of massive mimo with 2d active antenna array," in *Proc. IEEE GLOBECOM*, Dec. 2012, pp. 691–696.

[12] Q.-U.-A. Nadeem, A. Kammoun, M. Debbah, and M.-S. Alouini, "3D massive MIMO systems: Modeling and performance analysis," *IEEE Trans. Wireless Commun.*, vol. 14, no. 12, pp. 6926–6939, Dec. 2015.

[13] O. Elijah, C. Y. Leow, T. A. Rahman, S. Nunoo, and S. Z. Iliya, "A comprehensive survey of pilot contamination in massive MIMO–5G system," *IEEE Commun. Surveys Tuts.*, vol. 18, no. 2, pp. 905–923, 2nd Quar., 2016.

[14] X. Li, S. Jin, X. Gao, and R. W. Heath, Jr., "Three-dimensional beamforming for large-scale FD-MIMO systems exploiting statistical channel state information," *IEEE Trans. Veh. Technol.*, vol. 65, no. 11, pp. 8992–9005, Nov. 2016.

[15] E. Björnson, E. G. Larsson, and T. L. Marzetta, "Massive MIMO: Ten myths and one critical question," *IEEE Commun. Mag.*, vol. 54, no. 2, pp. 114–123, Feb. 2016.

[16] S. Zhang, A. Doufexi, and A. Nix, "Evaluating realistic performance gains of massive multi-user MIMO system in urban city deployments," in *Proc. 23rd Int. Conf. Telecommun.*, May 2016, pp. 1–6.

[17] W. Zhang *et al.*, "Field trial and future enhancements for TDD massive MIMO networks," in *Proc. IEEE PIMRC*, Aug. 2015, pp. 2339–2343.

[18] X. Wang *et al.*, "Large scale experimental trial of 5G mobile communication systems—TDD massive MIMO with linear and non-linear precoding schemes," in *Proc. IEEE PIMRC*, Sep. 2016, pp. 1–5.

[19] G. Liu, X. Hou, F. Wang, J. Jin, H. Tong, and Y. Huang, "Achieving 3D-MIMO with massive antennas from theory to practice with evaluation and field trial results," *IEEE System J.*, vol. 11, no. 1, pp. 62–71, Mar. 2017.

[20] *Evolved Universal Terrestrial Radio Access (E-UTRA), Physical Channels and Modulation*, 3GPP, document TSG RAN TS 36.211 v11.4.0, Sep. 2013.

[21] A. F. Molisch *et al.* (Sep. 2016). "Hybrid beamforming for massive MIMO—A survey." [Online]. Available: https://arxiv.org/abs/1609.05078

[22] A. Paulraj, D. A. Gore, R. U. Nabar, and H. Bolcskei, "An overview of MIMO communications—A key to gigabit wireless," *Proc. IEEE*, vol. 92, no. 2, pp. 198–218, Feb. 2004.

[23] Q. H. Spencer, A. L. Swindlehurst, and M. Haardt, "Zero-forcing methods for downlink spatial multiplexing in multiuser MIMO channels," *IEEE Trans. Signal Process.*, vol. 52, no. 2, pp. 461–471, Feb. 2004.

[24] G. Liu, X. Liu, and P. Zhang, "QoS oriented dynamical resource allocation for eigen beamforming MIMO OFDM," in *Proc. IEEE VTC-Fall*, Feb. 2005, pp. 1450–1454.

[25] Y. Xu, H. Yang, F. Ren, C. Lin, and X. Shen, "Frequency domain packet scheduling with MIMO for 3GPP LTE downlink," *IEEE Trans. Wireless Commun.*, vol. 12, no. 4, pp. 1752–1761, Apr. 2013.

[26] T. Yoo and A. Goldsmith, "On the optimality of multiantenna broadcast scheduling using zero-forcing beamforming," *IEEE J. Sel. Areas Commun.*, vol. 24, no. 3, pp. 528–541, Mar. 2006.

[27] *Study on 3D Channel Model for LTE (Release 12)*, 3GPP, document TSG RAN TR 36.873 v12.0.0, Sep. 2014.

Guangyi Liu received the Ph.D. degree from the Beijing University of Posts and Telecommunications. He was with Siemens and ALU working on 3G research and development for a few years. He is currently the CTO of the Wireless Department, China Mobile Research Institute, where he is in charge of the wireless technology research and development, including LTE/LTE-Advanced and 5G. He is very active in global industrialization activities, including acting as the Chair of Spectrum Working Group, GTI (Global TD-LTE Initiative), and the Vice-Chair of the CCSA, TC5, and WG6.

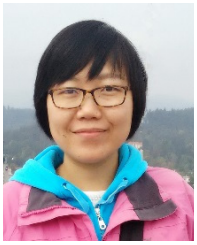

Xueying Hou received the Ph.D. degree in signal and information processing from Beihang University, China, in 2013. She is currently with the China Mobile Research Institute as a Standard Engineer, with a focus on the standardization of LTE/LTE-A and 5G. Her research interests include MIMO, cooperative communication, and channel acquisition techniques in wireless systems.

Jing Jin received the B.S. and Ph.D. degrees from the Beijing University of Posts and Telecommunications in 2006 and 2011, respectively. She is currently with the China Mobile Research Institute. Her research interests include wireless communications, MIMO, multiuser beamforming, and interference cancellation.

Fei Wang received the B.S. and M.S. degrees in electronic engineering from the Beijing University of Posts and Telecommunications in 2008 and 2011, respectively. In 2011, he joined the China Mobile Research Institute, where he is currently involved in the research, prototyping, and standardization of multiple antenna techniques in LTE/LTE-A and 5G. His research interests include multiple antenna techniques, coordination schemes, and advanced receivers for next generation systems.

Qixing Wang received the B.S. and Ph.D. degrees from the Beijing University of Posts and Telecommunications in 2004 and 2008, respectively. He is currently with the China Mobile Research Institute. His research interests include massive MIMO, multiuser beamforming, and interference cancellation.

Yue Hao received the B.S. and M.S. degrees in electronic information engineering from the Beijing University of Technology, Beijing, China, in 2013 and 2016, respectively. She is currently with the China Mobile Research Institute, Beijing. Her research interests include wireless communications and multiple antenna techniques.

Yuhong Huang received the degree from the Beijing University of Post and Telecom. She joined the China Mobile Research Institute in 1996, where she is currently the Deputy General Manager, where she is responsible for the work of wireless technology, terminal technology, test technology, and customer and market research. She has participated in several important projects, such as technical and strategic research, specification, test and trail of GSM900/1800, GPRS/EDGE, CMNet, WLAN, 3G, and LTE. She also leads the research and standardization work of LTE evolution and 5G. She served as the Vice-Chair of the 3GPP SA. She serves as a Steering Committee Member of the NGMN and the Secretary-General of the Global TD-LTE Initiative.

Xiaoyun Wang is currently the General Manager of Technical Department with China Mobile, the General Manager of the China Mobile Research Institute, and the Vice-Chairman of the IMT-2020, China's 5G Promotion Group. She is currently in charge of the medium and long-term technical planning of China Mobile, the build of technical innovation architecture, and the organization of the research and development work of China Mobile.

Xiao Xiao received the Ph.D. degree in electrical engineering from the HuaZhong University of Technology and Science in 2006. In 2008, he joined Huawei Technologies Co. Ltd., where he took charge of the innovation and product management of the new technologies, including LTE, 4.5G, and 5G, such as massive MIMO, distributed MIMO, UCN/UDN, UL capability enhancement, and cloud RAN.

Ailin Deng was the Head of TDD LTE Product Management, TDD LTE Solution Design, and CDMA Solution Design with Huawei Technologies Co. Ltd., where he is currently the Head of 5G Product Management. He has over 16 years of work experience on wireless product research and development and planning. He is a Principal Product Manager, who makes important contributions to Massive MIMO product planning, implementation, and industry promotion.